Chemical Engineering Journal 147 (2009) 356–365

Contents lists available at ScienceDirect

Chemical Engineering Journal

journal homepage: www.elsevier.com/locate/cej

Procedures for heat recovery in the catalytic combustion of lean methane–air mixtures in a reverse flow reactor

Pablo Marín, Salvador Ordóñez*, Fernando V. Díez

Department of Chemical Engineering and Environmental Technology, University of Oviedo, Facultad de Química, Julián Clavería 8, Oviedo 33006, Spain

ARTICLE INFO

Article history:
Received 5 September 2008
Received in revised form 9 November 2008
Accepted 25 November 2008

Keywords:
Catalytic afterburners
Dynamic simulation
Hydrocarbon emissions
Reactor stability
Steam generation

ABSTRACT

The performance of different heat recovery strategies for reverse flow catalytic reactors, considering both the gas extracting point (centre or end) and the possibility of returning the cooled gases, has been studied in this work. The study was carried out by means of simulations of the combustion of methane over a monolithic Pd-catalyst using a heterogeneous 1D dynamic model. The effect of methane feed concentration (3000–9000 ppmV), has also been considered. The withdrawal of the hot gases from the end of the catalytic bed without returning the cooled gases has been shown to provide the most stable performance, whereas the extraction of the gases from the central part of the bed severely affects reactor performance. Finally, the amount of high-pressure steam that can be generated using the best heat recovery method has been also estimated.

1. Introduction

Methane is the second most important greenhouse gas, after carbon dioxide. Its main anthropogenic sources are livestock, landfills, natural gas and oil extraction and distribution systems, and coal mines. Since the global warming potential of methane is about 23 times higher than the corresponding to carbon dioxide, there is a clear advantage in transforming methane to carbon dioxide. Moreover, depending on the emission, methane concentration, and the selected treatment method, it is possible to recover an important fraction of the heat released in the reaction, generating high-pressure steam or electricity [1–3].

Catalytic combustion reduces considerably the ignition temperature in comparison to homogeneous combustion, resulting in operational advantages such as lower pressure drops and heat losses, requirement of smaller equipments, and negligible production of nitrogen oxides [4]. Besides the industrial importance of methane combustion, methane is commonly used as model compound in catalytic combustion research, because it is more difficult to burn than most of the hydrocarbons, or volatile organic compounds (VOCs) in general [5,6]. In order to avoid the consumption of fuel in the feed pre-heating up to the ignition temperature, or even recover a fraction of the combustion heat, different heat integration techniques have been proposed, being reverse flow reactors (RFRs) one of the most promising [7,8].

Reverse flow reactors belong to the group of chemical reactors that work under forced unsteady state conditions. RFRs consist of a fixed catalytic bed, and the unsteady-state behaviour is generated by periodically reversing the feed flow direction through the bed. RFRs take advantage of the velocity difference between the flowing gas and the temperature front moving through the catalyst bed. By selecting an appropriate reversing switching time, it is possible to keep inside the reactor the high-temperature plateau generated by the combustion heat released. Therefore, autothermal operation is possible even when working with cold lean feeds, because the heat released in the reaction is stored inside the reactor in consecutive cycles. Both ends of the reactor usually remain below the ignition temperature, so this part of the bed commonly contains inert material with suitable physical properties, instead of catalyst. The system is started by pre-heating the reactor bed above the ignition point. Once the feed flow reversing is started, the preheating can be disconnected, as no additional heat is needed. After several cycles, a pseudo-steady state is reached, in which temperature and concentration profiles are repeated between cycles. For more details about RFR, see the reviews of Matros and Eigenberger [9,10].

The heat released by the reaction is accumulated in the centre of the RFR, where the temperature increases up to the pseudo-steady-state value, which depends on feed concentration and reversing switching time. The great RFR heat integration capability allows not only the operation without additional fuel consumption, but also, in several cases, the recovery of some of the heat released by the reaction. Different strategies have been proposed and studied in the literature for this purpose, such as heat transmission through the reactor wall [11,12], introduction of a heat exchanger in the middle

Abbreviations: RFR, reverse flow reactor; VOC, volatile organic compound.

* Corresponding author. Tel.: +34 985 103 437; fax: +34 985 103 434.
E-mail address: sordonez@uniovi.es (S. Ordóñez).

1385-8947/$ – see front matter © 2008 Elsevier B.V. All rights reserved.
doi:10.1016/j.cej.2008.11.041

Nomenclature

List of symbols

a_G	$(4/D_H)$, surface–gas volume ratio (m^2/m^3)
a_S	$(4/D_H)\varepsilon/(1-\varepsilon)$, surface–solid volume ratio (m^2/m^3)
b	exponent of the kinetic equation
C_P	heat capacity (J/(kg K))
$\langle d_{pore}\rangle$	washcoat mean pore diameter (m)
D_{eff}	axial mass dispersion coefficient (m^2/s)
D_H	hydraulic diameter (m)
D_R	reactor diameter (m)
F	molar flow rate (mol/s)
h	gas–solid heat transmission coefficient (W/(m^2 K))
ΔH_R	combustion enthalpy (J/mol)
k_{eff}	axial heat dispersion coefficient (W/(m K))
k_m	kinetic constant per catalyst mass based on partial pressures (mol/(s kg $Pa^{1.5}$))
K_G	gas–solid mass transfer coefficient (m/s)
L_R	reactor length (m)
L_W	washcoat thickness (m)
m_v	amount of high-pressure steam (kg/s)
M_G	total gas molecular weight (kg/mol)
P	pressure (Pa)
Q_{extr}	heat recovered in the heat exchanger (MW)
Q_G	gas flow rate (m^3/s)
Q_{tot}	$\Delta H_R y_{G0} F_{tot}$, total amount of heat released by the reaction (MW)
r_m	reaction rate per unit of catalyst mass (mol/(s kg))
R	ideal gas constant (J/(mol K))
t	time (s)
t_{sw}	switching time (s)
T	temperature (K)
T_C	temperature of the cold gas returning the reactor (K)
ΔT_{ad}	$(\Delta H_R y_{G0})/(C_{PG} M_G)$, adiabatic temperature rise (°C)
ΔT_C	temperature difference in the heat exchanger (K)
u	surface gas velocity (m/s)
v	lineal gas velocity (m/s)
X	conversion
y	molar fraction in the gas phase
z	axial length along the reactor (m)

Greek symbols

ε	bed void fraction
η	internal mass transfer effectiveness factor
η_{th}	Q_{extr}/Q_{tot}, heat recovery efficiency
κ	thermal conductivity (W/(m K))
ρ	density (kg/m^3)
τ_{pore}	internal catalyst tortuosity
ϕ	fraction of hot gas removed

Sub indexes and super indexes

C	catalyst
f	conditions at the hot gas withdrawal point
G	gas phase
I	inert
max	maximum
S	solid phase
tot	total
0	reactor inlet conditions

of the catalytic bed [2,13–15], or hot gas withdrawal from the middle of the reactor [2,14,16,17]. The two former strategies can cause, depending on the operating conditions, a marked asymmetry in the reactor behaviour, with negative effects on reactor performance [2]. On the other hand, when hot gas is withdrawn from the middle of the reactor, the effective conversion decreases, due to the unreacted methane extracted with the hot gases. This effect can be overcome by oversizing the catalytic bed, so that the required feed conversion is achieved after crossing half catalytic bed.

In this work, a detailed study of the heat recovery capabilities of RFR used for the combustion of lean methane emissions is performed. The two most important heat recovery methods, hot gas withdrawal and heat exchange with cold gas returning, are considered and compared to each other. In order to face the problem of un-reacted methane emissions associated with hot gas withdrawal, an improved layout, using a hot gas extracting point different from the classical middle reactor bed, is proposed in this work. The performance of this new layout is compared with the classical one, for the two methods of heat recovery considered.

This study is performed by means of RFR simulations, using a 1D heterogeneous dynamic model, presented in Appendix A. The reactor is considered to be formed by three monolith beds: two inert beds at the ends, and a catalytic bed in the middle. Therefore, the advantages of the monolith beds are entirely exploited [5,18].

2. Methods of heat recovery

Two methods of heat recovery from a RFR are studied in this work. The so-called method 1 consists of withdrawing part of the hot gas stream from the reactor to recover heat in an external heat exchanger; this stream does not return to the reactor. Method 2 consists of withdrawing the whole hot gas stream out of the reactor, recovering part of its heat content in an external heat exchanger, and then returning it to the reactor. In addition, two different layouts, depending on the hot gas extracting point, are considered for each method. The classical hot gas extracting point is the middle of the reactor (layout A), because the temperature in this zone is higher, and hence a higher heat recovery efficiency can be achieved. The alternative layout proposed here (layout B) extracts the hot gas in a point situated after the catalyst bed, in the flow direction. Therefore, the need of over-sizing the catalytic bed can be eliminated, very low amounts of un-reacted methane being emitted. This topic has been scarcely considered in the literature [13].

Fig. 1 shows the schemes of the four proposed configurations (1A, 1B, 2A and 2B, corresponding to combinations of methods 1 and 2, and layouts A and B). Schemes for method 1 include control valves, required to regulate the amount of hot gas withdrawn. For B layouts, the extraction point changes every the half-cycle, being always situated at the corresponding end of the catalytic bed. Fig. 1(c), corresponding to configuration 1B and half-cycle with flow from top to bottom, shows valves V1 closed and V2 partially open, so that hot gas is extracted after crossing the catalytic bed. For half-cycles with flow from bottom to top, valve configuration is the opposite. For configuration 2B (Fig. 1(d)), the layout is more complex, because the cooled gas stream returns to the reactor. In this case, the use of 3 three-way valves synchronized with the flow reversing valves is necessary.

3. Heat recovery case study

For illustration of the different configurations proposed, the treatment of a 100 m^3/s lean methane–air mixture at 25 °C and 101 kPa is considered. Since methane inlet concentration determines the amount of heat released in the reactor, and hence the maximum heat extracted, four different concentrations, ranging from 3000 to 9000 ppmV, have been selected for comparison. These values are within the range of typical coal mine ventilation air emissions, where a single ventilation shaft can discharge from 75 to 275 m^3/s of air with methane concentrations ranging from 0.1 to

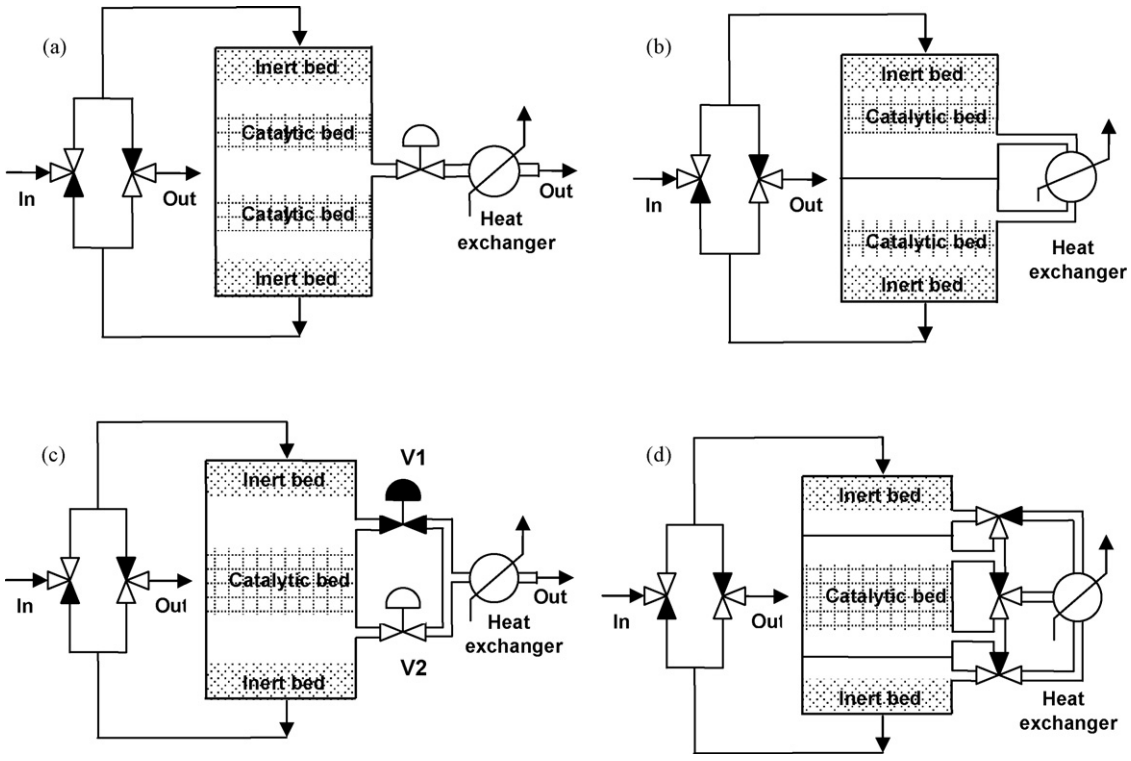

Fig. 1. Schemes of the different configurations for heat recovery from RFR: (a) configuration 1A; (b) configuration 2A; (c) configuration 1B; (d) sonfiguration 2B. Valve in black indicates closed.

1 vol.%, depending on the geological characteristics and the daily activity of the mine (typical average concentration 0.4 vol.%) [2,3].

The operation conditions and the most important properties, for which the mathematical model is solved, are shown in Table 1. The surface velocity is fixed to 1 m/s, which has been found to be a value close to the optimum for RFR [19,20]. Regarding the switching time, since this parameter determines the heat stored in the reactor between cycles, it is very important to compare the different heat recovery alternatives keeping it constant. A high value of the switching time leads to larger reactors, although the system increases its capability to overcome disturbances in the feed concentration. However, very low-switching times increase the contribution of washout (emission of un-reacted methane contained in the inert beds due to the flow reversal) [21]. As a result, a value of 300 s has been set as appropriate [7,19–21].

Table 1
Operation conditions and catalyst and inert bed properties.

Operation conditions	
Inlet gas flow rate, Q_{G0}	100 m^3/s
Inlet gas temperature, T_{G0}	25 °C
Inlet methane concentration, y_{G0}	3000/5000/7000/9000 ppmV
Superficial velocity, u_0	1 m/s
Catalytic bed fraction	50% (vol.)
Switching time, t_{sw}	300 s
Catalyst properties	
Cell density	370 cpsi
Bed void fraction, ε	0.54
Hydraulic diameter, D_H	1×10^{-3} m
Density, ρ_C	2000 kg/m^3
Heat capacity, $C_{P,C}$	900 J/(kg K)
Thermal conductivity, κ_C	1 W/(m K)
Washcoat thickness, L_W	9×10^{-5} m
Washcoat mean pore diameter, $<d_{pore}>$	6.8×10^{-9} m
Washcoat internal porosity, ε_{pore}	0.12
Pore tortosuity, τ_{pore}	2
Inert properties	
Cell density	200 cpsi
Bed void fraction, ε	0.605
Hydraulic diameter, D_H	1.4×10^{-3} m
Density, ρ_I	2000 kg/m^3
Heat capacity, $C_{P,I}$	900 J/(kg K)
Thermal conductivity, κ_I	1 W/(m K)

The properties of the catalyst and inert monoliths shown in Table 1 have been obtained experimentally using commercial monoliths, being in the range of typical catalysts employed in catalytic combustion. The hydraulic diameter and the washcoat thickness have been determined using a stereomicroscope, whereas the washcoat mean pore diameter and internal porosity have been calculated from BET analysis.

4. RFR design

Before performing the heat recovery study, specific RFRs were designed for each feed methane concentration considered. Thus, the heat recovery efficiency is evaluated and compared for the different resulting designs, broader conclusions being obtained. The RFR design consists on the calculation of the reactor length that provides 99.99% outlet pseudo-steady-state average methane conversion. The reactor is designed using the RFR mathematical model (see Appendix A) and the parameters given in Table 1. Since the reactor length is an implicit parameter of the mathematical model, the reactor length is calculated by trial and error, solving the model up to the pseudo-steady state (50 cycles are usually enough) for different values of the reactor length. Further details about the reactor modelling, as well as experimental validation are provided in previous papers [19–22].

Fig. 2 shows the average outlet conversion and maximum reactor temperature as a function of reactor length for the different feed methane concentrations considered (each point of the plots corresponds to a pseudo-steady-state value). A sharp decrease in conversion (Fig. 2(a)) is observed when reactor extinction takes place. Reactor lengths corresponding to extinction (0% conversion)

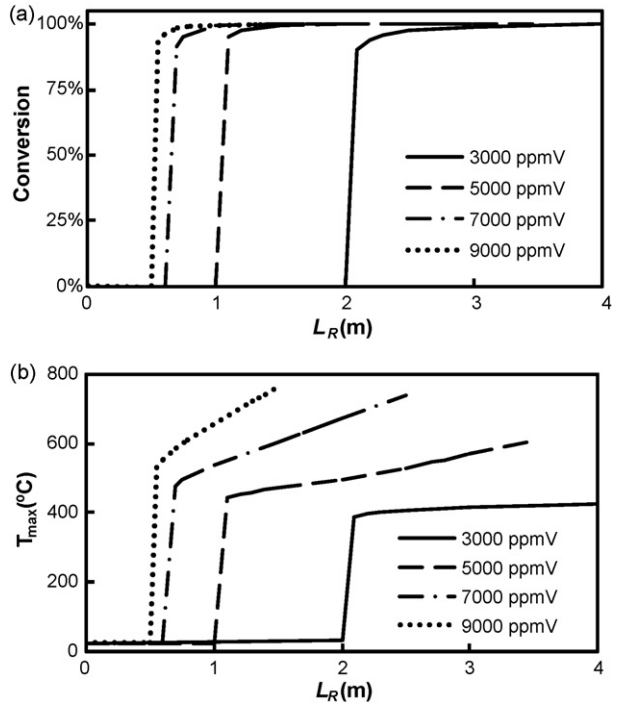

Fig. 2. Average outlet conversion (a) and maximum solid temperature (b) as a function of reactor length, for the combustion of methane without heat recovery for different methane concentrations.

and 99.99% conversion are summarised in Table 2. Both magnitudes decrease as feed methane concentration increases, since higher heat amounts are released by combustion, increasing the maximum temperature inside the reactor (Fig. 2(b)), and hence reaction rate. Increases in the hydrocarbon concentration in the feed lead to marked increases of the reactor stability, allowing stable operation with lower reactor lengths. Consequently, the performance of the reactor with different methane concentrations will be characterised in terms of the length needed for a 99.99% of conversion (Fig. 2(a)).

5. Results and discussion

The feasibility of heat recovery in the four proposed RFR-heat exchanger configurations is analysed for the case study and different methane inlet concentrations. Reactor performance and heat extraction capacity are evaluated by means of simulations. For each heat recovery method, the reactor performance is studied by varying the amount of heat extracted from the system (Q_{extr}). The maximum amount of heat that can be extracted from the reactor (Q_{tot}) is the heat released by the reaction, which depends only on the feed flow rate and methane concentration (see Table 2). Obviously, since reactor thermal efficiency is not 100%, only part of Q_{tot} can be recovered from the reactor. This part, Q_{extr}, is the amount of heat recovered in the heat exchanger, given by Eq. (1) for method 1 and Eq. (2) for method 2:

$$Q_{extr} = \phi F_{tot} \int_{(T_G)_{0^-}}^{(T_G)_{z=l^-}} C_{PG}\, dT_G \quad (1)$$

$$Q_{extr} = F_{tot} \int_{(T_G)^{in}_{z=l^-}}^{(T_G)^{out}_{z=l^-}} C_{PG}\, dT_G \quad (2)$$

As shown in Eq. (1), the amount of heat extracted in method 1 depends on the fraction of hot gas removed (ϕ), so this variable is chosen to conduct the heat recovery study. For method 2, two variables have been selected, as proposed by Gosiewski and Warmuzinski [2], the temperature of the cold gas returning to the reactor (T_C), and the temperature decrease of the hot stream in the heat exchanger (ΔT_C). Both variables are related to each other, but due to the dynamic evolution of the reactor, the selection of one or another to control the heat extracted can result in different reactor performance.

RFR performance is measured in terms of average outlet conversion ($\langle X_{out} \rangle$) and maximum bed temperature (T_{max}), both calculated by simulation. The maximum solid temperature is very important in RFR operation, because too high temperatures can cause catalyst deactivation, resulting in the progressive reactor extinction [23]. Heat extraction capacity is mainly determined using the heat recovery efficiency (η_{th}), defined as the ratio between the heat extracted and the maximum heat that can be removed from the reactor ($\eta_{th} = Q_{extr}/Q_{tot}$).

5.1. Method 1

Figs. 3 and 4 compare the performance of configurations 1A and 1B. The most significant difference is that configuration 1A exhibits lower stability, as the fraction of hot gas removed increases, for all methane feed concentrations. For configuration 1A (Fig. 3(a) and (c)), as the fraction of gas removed (or the heat extracted from the reactor) increases, the maximum temperature decreases up to reactor extinction (conversion suddenly decreases to zero). Stable operation is possible for higher methane feed concentrations and higher fractions of gas removed, because more heat is released in the reaction. A better performance of configuration 1B is observed in Fig. 3(b) and (d). Although, both outlet conversion and maximum temperature decrease as the fraction of gas removed increases, extinction does not take place at the studied conditions. In this configuration, only the regeneration capacity of the following inert end is affected, since the gas is extracted after the catalytic bed, instead of the middle point of the reactor, and hence presents lower heat storage capacity). As a result, stable operation with high conversion (more than 98%) is possible for configuration 1B.

The heat extraction capacity of both configurations is compared in Fig. 4. For low fractions of hot gas removed, configuration 1A presents slightly higher heat recovery efficiencies. In configuration 1A the gas is removed from the centre of the reactor, which is at higher temperature than the point at which the gas is withdraw in configuration 1B, resulting in a higher heat extraction capacity. Despite of this, configuration 1B provides better reactor stability, and allows operation with high fraction of gas removed, resulting then in higher heat recovery efficiencies than configuration 1A.

In conclusion, the operation of configuration 1A is highly affected by the heat recovery, reducing considerably the stable operating range. In contrast, configuration 1B can maintain the reactor ignited with high-outlet conversions, for a wide range of fraction of hot gas removed. As result, layout B is suggested as a better alternative for heat extraction based on method 1.

Table 2
Results of the RFR design for different inlet methane concentrations.

y_{G0} (ppmV)	ΔT_{ad} (°C)	Q_{tot} (MW)	$L_{R,X=0\%}$[a] (m)	$L_{R,X=99.99\%}$[b] (m)	T_{max} (°C)
3000	83	9.8	2.1	6.2	467
5000	138	16.4	1.1	2.7	546
7000	194	23.0	0.7	1.7	631
9000	249	29.5	0.55	1.35	733

[a] Reactor length corresponding to extinction.
[b] Reactor length corresponding to 99.99% conversion.

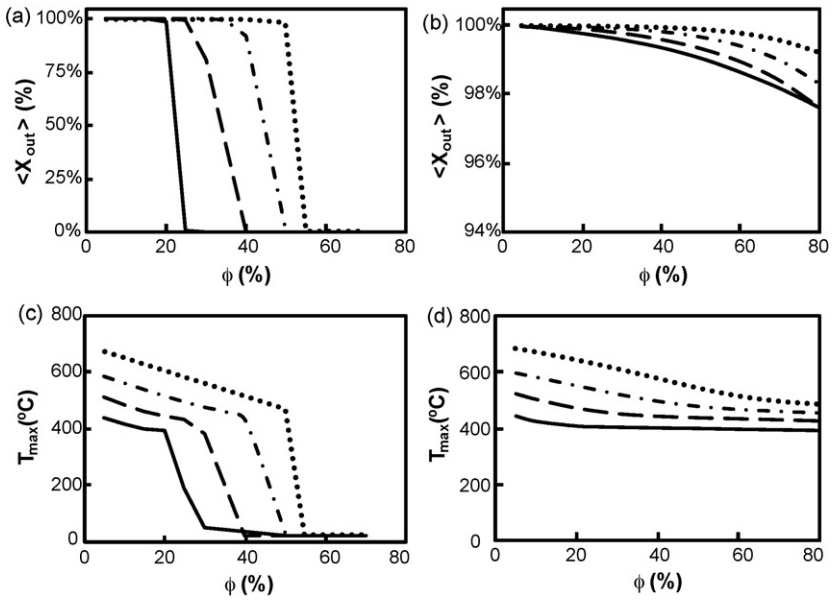

Fig. 3. Evaluation of heat recovery by method 1. Average outlet conversion: (a) configuration 1A, (b) configuration 1B. Maximum solid temperature: (c) configuration 1A, (d) configuration 1B. (—) 3000 ppmV, (– – –) 5000 ppmV, (- · -) 7000 ppmV, (· · ·) 9000 ppmV.

5.2. Method 2

The performance of method 2, based on recovering heat from the whole hot gas stream, has been evaluated using two variables: the temperature of the cold gas returning the reactor (T_C), and the temperature decrease of the hot stream in the heat exchanger (ΔT_C) [2]. T_C determines the heat returned to the reactor, whereas ΔT_C determines the amount of heat recovered. The relationship between these two variables and the simulated variables calculated from the reactor mathematical model are shown in Appendix A. In this work, both variables are used in the study, which allows a broader evaluation of the performance of method 2, as shown by Gosiewski and Warmuzinski [2].

The behaviour of the reactor as a function of the returning gas temperature (T_C) is depicted in Figs. 5–7. Conversion decreases as T_C decreases (Fig. 5(a) and (b)) because lower heat amounts are allowed to return to the reactor. Configuration 2A exhibits worse performance, with lower methane conversion and extinction for low-T_C values. The advantages of layout B for method 2 are similar to the advantages discussed for method 1, but even more pronounced in this case, because of the negative effect of the cold gas returned to the reactor. For configuration 2A, reaction extinction can occur when temperature of the returned stream is too low. This effect is less pronounced in configuration 2B, because heat extraction affects mostly the exit inner bed, the catalyst bed remaining at high temperature.

The evolution of T_{max} with T_C for configuration 2B follows the expected trend of decreasing T_{max} for decreasing T_C (Fig. 5(d)). However, the behaviour for configuration 2A is more complex (Fig. 5(c)): initially, on decreasing T_C, the expected decreasing tendency is observed, but for $T_C < 300\,^{\circ}C$, T_{max} increases—reaching a maximum, and then decreases again. This behaviour is caused by a change in the pseudo-steady-state behaviour of the reactor. For low amounts of heat extracted ($T_C > 300\,^{\circ}C$), a symmetric behaviour is observed, the evolution of temperature and concentration profiles of the direct and reverse half-cycles being similar. This fact leads to higher catalytic bed temperatures, ensuring that all the catalyst is used for the reaction. For higher fraction of heat extracted ($T_C < 300\,^{\circ}C$), half of the catalytic bed remains always at low temperature, reaction taking place only in the other half (Fig. 6). The heat of reaction is then released in half of the catalytic bed, and do not spread along all the bed, resulting in a noticeable increase of the pseudo-steady-state maximum temperature. This behaviour is illustrated in Fig. 6 for two different temperatures of the returning gas, 250 and 350 °C. This kind of complex dynamic features affecting the pseudo-steady-state behaviour of cooled RFR has been studied by Khinast et al. [11,12]. This complex behaviour is not observed for methane feed concentration of 3000 ppmV, as shown in Fig. 5(c), because for such low-feed concentrations, the heat released in the reaction is lower and is progressively spread along the reactor length, avoiding the accumulation of heat in half of the catalytic reported in Fig. 6.

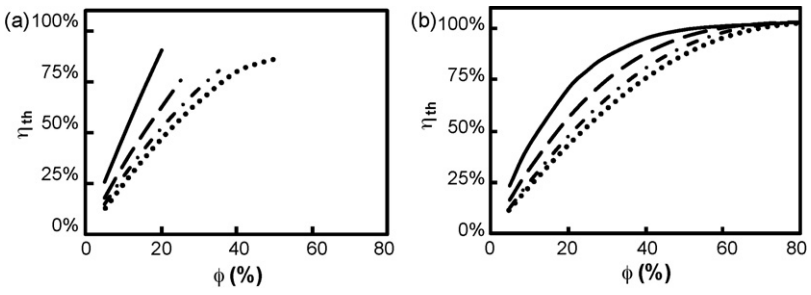

Fig. 4. Evaluation of heat recovery by method 1. Heat recovery efficiency: (a) configuration 1A, (b) configuration 1B. (—) 3000 ppmV, (– – –) 5000 ppmV, (- · -) 7000 ppmV, (· · ·) 9000 ppmV.

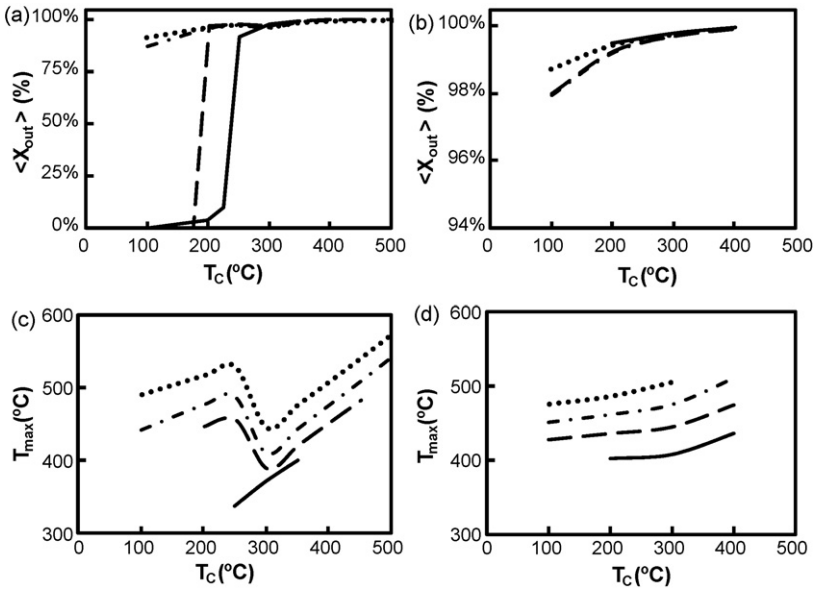

Fig. 5. Evaluation of heat recovery by method 2: effect of the temperature of the returning gas. Average outlet conversion: (a) configuration 2A, (b) configuration 2B. Maximum solid temperature: (c) configuration 2A, (d) configuration 2B. (—) 3000 ppmV, (– – –) 5000 ppmV, (- · -) 7000 ppmV, (· · ·) 9000 ppmV.

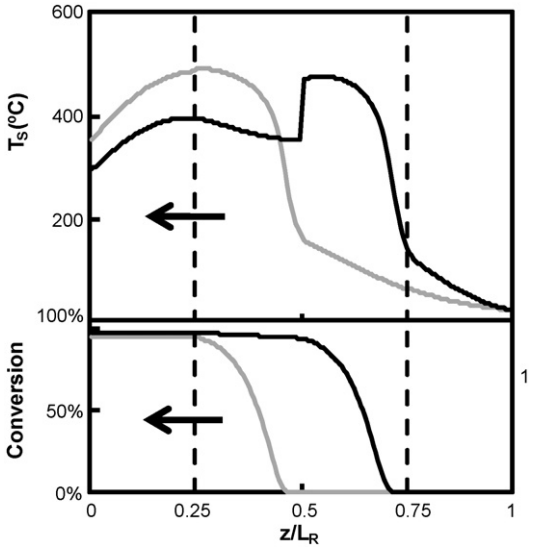

Fig. 6. Conversion and temperature profiles for configuration 2A at the end of a reverse half-cycle (the direction of the flow is indicated by an arrow). 9000 ppmV methane. Effect of the temperature of the returning gas: ( ) T_C = 250 °C, (—) T_C = 350 °C.

The complex dynamic behaviour reported for configuration 2A and T_C < 300 °C can also be observed for the heat recover efficiency plot (Fig. 7(a)). Thus, heat recovery efficiency increases sharply for T_C < 300 °C (explained by the increase of the maximum temperature of the catalytic bed observed in Fig. 5(c)), causing an increase of the temperature of the hot gas withdrawn. However, despite the high-heat recovery efficiencies observed, operation for T_C < 300 °C is not recommended, since only a minor part of the catalyst is being effectively used. Regarding configuration 2B (Fig. 7(b)), on decreasing T_C, a regular increase in the heat recovery efficiency is observed. When comparing the heat recovery efficiency of configurations 2A and 2B, it is observed that configuration 2B performs better for T_C > 300 °C, whereas for configuration 2A operation is not recommended for T_C < 300 °C. As a result, layout B is the best option to carry out the heat extraction, as found previously for method 1.

Figs. 8 and 9 show a comparison of the configurations 2A and 2B in terms of the temperature cooling difference (ΔT_C). According to these plots, higher heat amounts are recovered in the heat exchanger as ΔT_C increases, resulting in a lower maximum reactor temperature, and hence lower conversions. Results are qualitatively similar to the ones obtained when comparing the configurations in terms of T_C. Configuration 2A exhibits reactor extinction for values of ΔT_C in the range 30–100 °C, depending on the methane feed concentration, while configuration 2B performs well, with only a decrease in the average outlet conversion for ΔT_C 150–300 °C. For configuration 2B, the gas is extracted and returned to the reactor

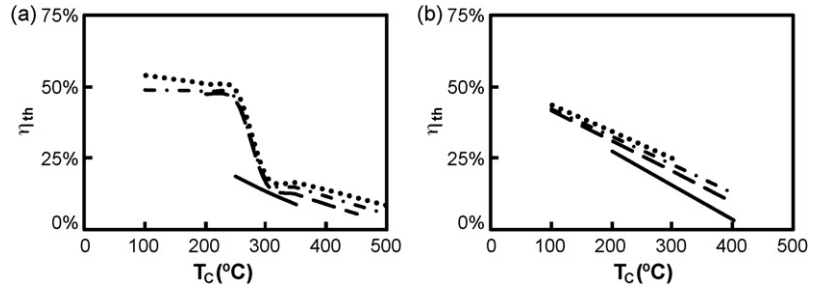

Fig. 7. Evaluation of heat recovery by method 2: effect of the temperature of the returning gas. Heat recovery efficiency: (a) configuration 2A, (b) configuration 2B. (—) 3000 ppmV, (– – –) 5000 ppmV, (- · -) 7000 ppmV, (· · ·) 9000 ppmV.

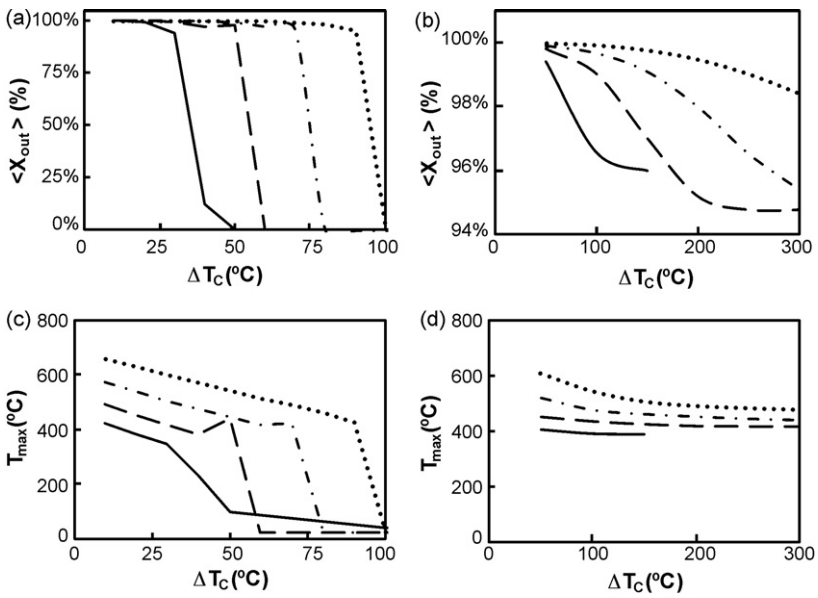

Fig. 8. Evaluation of heat recovery by method 2: effect of the temperature cooling difference. Average outlet conversion: (a) configuration 2A, (b) configuration 2B. Maximum solid temperature: (c) configuration 2A, (d) configuration 2B. (—) 3000 ppmV, (– – –) 5000 ppmV, (- · -) 7000 ppmV, (· · ·) 9000 ppmV.

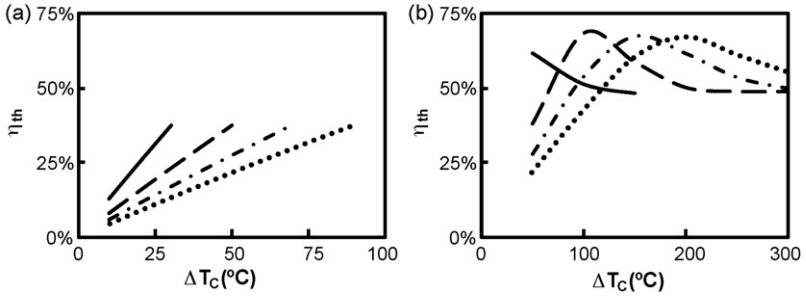

Fig. 9. Evaluation of heat recovery by method 2: effect of the temperature cooling difference. Heat recovery efficiency: (a) configuration 2A, (b) configuration 2B. (—) 3000 ppmV, (– – –) 5000 ppmV, (- · -) 7000 ppmV, (· · ·) 9000 ppmV.

after crossing the catalytic bed, so that the disturbances caused by the heat extraction only affect the inert end. Therefore, stable operation is possible for configuration 2B, even for high values of ΔT_C. However, operation with very high values of ΔT_C (high-heat extraction capacities) is not recommended for long periods of time, as the inert beds would remain at very low temperature during all the cycle. Anyway, configuration 2B is very interesting for maintaining the reactor ignited when disturbances on the feed concentration are common. For example, consider a RFR treating 7000 ppmV of methane and working with $\Delta T_C = 65\,^{\circ}C$. If the feed methane concentration is reduced to 3000 ppmV, and ΔT_C remains constant, the reactor will extinguish for configuration 2A, as shown in Fig. 8(a), while for configuration 2B only a small decrease in conversion will be observed (Fig. 8(b)).

Regarding the heat recovery efficiency (Fig. 9), a linear dependence on ΔT_C is observed for configuration 2A, being 40% the maximum heat recovery efficiency achieved for all the concentrations studied. Configuration 2B exhibits a maximum in the heat recovery efficiency, which takes place at lower ΔT_C for decreasing methane concentrations. However, the maximum is not observed for 3000 ppmV methane. The maximum corresponds to around 70% of heat recovery efficiency.

5.3. Comparison of methods 1 and 2

In this section the performance of methods 1 and 2 using layouts A and B is compared. Table 3 summarizes the most important results from the previous sections. The scope is to optimize the extraction of heat from the RFR, affecting as less as possible its stability. From the heat recovery efficiency plots (Figs. 4, 7 and 9), it can be observed that method 1 presents higher heat recovery efficiencies than method 2. The disturbance on the RFR behaviour produced by the heat extraction can also be analysed from the reactor temperature profiles. Similar temperature profiles have been observed for feed methane concentrations from 5000 to 9000 ppmV, being the

Table 3
Summary of the effects on main operation parameters of the reactor stability and heat recovery efficiency for the cases studied in this work.

Configuration	Stability ($\langle X_{out} \rangle$)	Heat recovery (η_{th})
1A	Strong dependence on ϕ and y_{G0}	Higher for the same ϕ values
1B	Weak dependence on ϕ	Higher at the highest values of ϕ
2A—T_C	Complex dynamic behaviour observed	Affected by this complex dynamic behaviour
2B—T_C	Weak dependence on T_C	Linear dependence on T_C
2A—ΔT_C	Linear dependence on y_{G0}	Linear dependence on ΔT_C
2B—ΔT_C	Weak dependence on ΔT_C	Existence of a maximum at different ΔT_C depending on inlet concentration

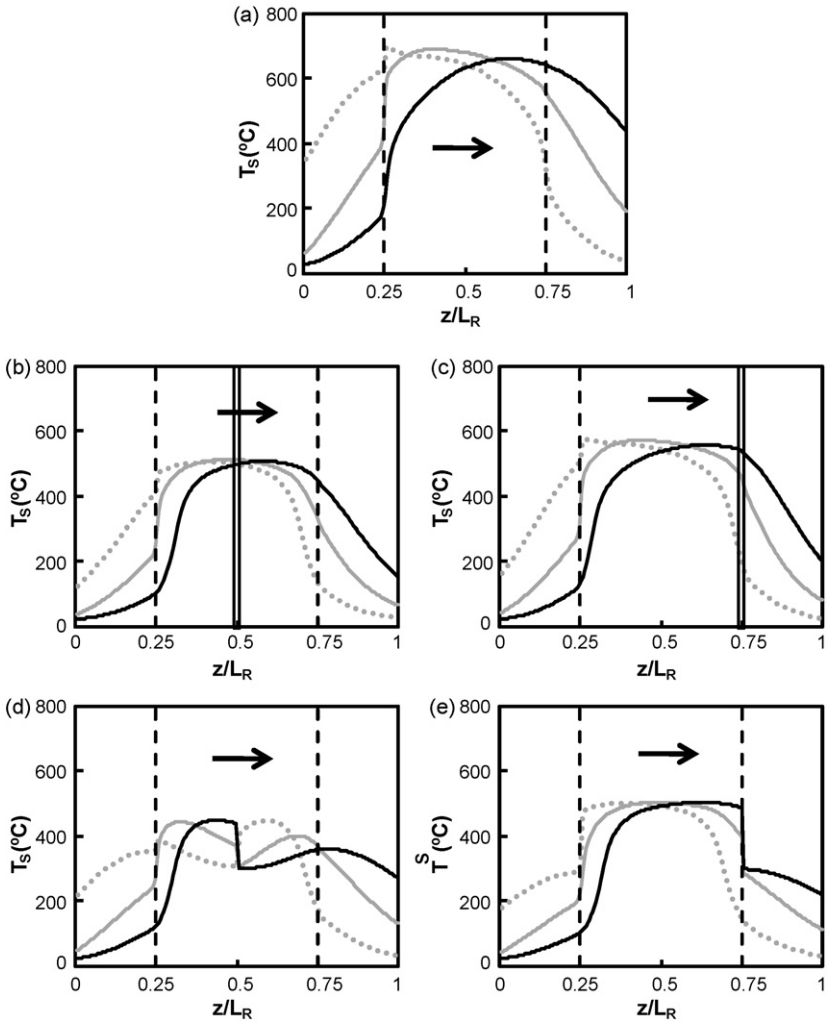

Fig. 10. Temperature profiles for 9000 ppmV methane feed concentration. (a) Without heat extraction. Method 1 (ϕ = 40%): (b) configuration 1A, (c) configuration 1B. Method 2 (T_C = 300 °C): (d) configuration 2A, (e) configuration 2B. Half-cycle with flow from left to right at the pseudo-steady state. The heat extracting point is marked in the plots by a double line. (• • •) beginning; (▬▬) middle; (—) end.

value of 9000 ppmV selected, because of its higher practical interest (case study with higher heat extraction potential). For illustrative purposes, Fig. 10 shows temperature profiles of the solids contained in the reactor at the beginning, middle, and end of a half-cycle with flow from left to right, with and without performing heat extraction. First, it is observed that, as expected, heat extraction reduces the temperature in the reactor. For relatively high-methane concentrations, maximum bed temperature without heat extraction (Fig. 10(a)) can be too high (around 700 °C in this case), which can be above the thermal stability limit of the catalyst [21]. In this case, heat extraction withdraws the remainder heat from the reactor, reducing the possibility of damaging the catalyst due to thermal deactivation.

Configurations 1A and 1B are compared for the same fraction of hot gas withdrawn (ϕ = 40%) (Fig. 10(b) and (c)). Temperature profiles are parabolic, with a high-temperature plateau occupying most of the catalytic bed in both cases. Profile for configuration 1B shows a higher and wider temperature plateau than configuration 1A, which explains the best stability provided by configuration 1B [23]. Configurations 2A and 2B are compared for a fixed returning gas temperature (T_C = 300 °C). The return of cold gas to the reactor produces an important disturbance in the temperature profile. This disturbance occurs in the middle of the catalyst bed for configuration 2A, which breaks the temperature plateau, reducing considerably the reactor stability. Moreover, the heat extraction efficiency (Fig. 7(a)) is quite low compared with the other configurations. Regarding configuration 2B, since hot gas extraction and return takes place at the end point of the catalytic bed in the direction of the flow, the temperature plateau in the catalyst bed is not disturbed and occupies most of the central part of the reactor.

Summarizing, hot gas extraction at the exit of the catalyst bed (layout B) has been found to be better than the extraction from the reactor middle point (layout A). When comparing the performance of the heat extraction methods, method 1 (cold gas is not returned to the reactor) performs better than method 2 (cold gas is returned), as heat extraction causes fewer disturbances to the reactor, and higher heat recovery efficiencies are possible for method 1 (Table 3).

5.4. Capacity of steam generation

In this section, another aspect of heat recovery from RFR is studied, the amount of high-pressure steam that can be generated from the heat extracted. Only method 1, the most efficient according to the results in the previous section, is considered here.

Calculations are done assuming counter-current heat transfer in the heat exchanger of Fig. 1, between the hot air withdrawn from the reactor, and the water/steam. Water is considered to enter at 60 °C and the steam is generated at 400 °C and 4 MPa. The temperature of the hot air entering the heat exchanger is calculated from the simulations of the RFR model of Appendix A. The calculations

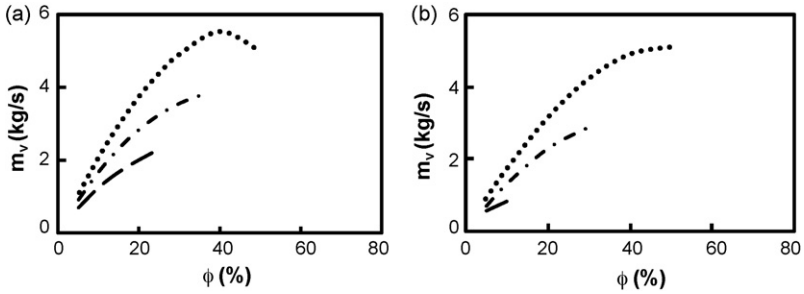

Fig. 11. Amount of high-pressure steam generated: (a) configuration 1A, (b) configuration 1B. (– – –) 5000 ppmV, (- · -) 7000 ppmV, (· · ·) 9000 ppmV.

of the amount of steam generated (m_v) are performed using the simulation software HYSYS (Aspentech). A minimum temperature approach between the cold and hot streams of the heat exchanger of 20 °C is also assumed in the calculation. Therefore, temperature crossing is avoided inside the heat exchanger, and a reasonable heat transfer area will result.

Fig. 11 shows the amount of steam generated for the different methane feed concentrations and fractions of hot gas removed considered. As expected, the amount of steam generated increases as methane feed concentration and fraction of hot gas removed increase (except for configuration 1A, 9000 ppmV methane and $\phi > 40$). The amount of steam produced is slightly higher for configuration 1A, due to its higher heat recovery efficiency, but the difference with configuration 1B is very small, and does not compensate the advantages of configuration 1B in terms of stability.

6. Conclusions

The comparison of the four different configurations for heat recovery from the combustion of lean methane mixtures in RFR, indicates that withdrawing hot gas from the end of the catalytic bed affects the RFR stability in lower extent than withdrawing the hot gas from the reactor centre. In the same way, the method consisting on withdrawing part of the hot gas from the reactor to recover the heat with no return of the cold gas, presents stability advantages when compared with the method consisting on withdrawing and returning to the reactor the whole extracted gas stream. The configuration consisting in withdrawing part of the hot gas from the catalytic bed end, with no return of the cool gas, provides the most stable RFR operation, and allows high-heat recovery efficiencies, maintaining very high-methane conversions.

Acknowledgements

This work was financed by a Research Project of the Regional Plan for Research, Development and Innovation of the Regional Government of Asturias (Spain) (FC03-PB02-133 and IB05-103).

Appendix A. Mathematical model

The simulations performed in this work have been done using an 1D heterogeneous dynamic model for RFR. This model was found to present a good equilibrium between accuracy and complexity, as demonstrated elsewhere for the combustion of methane, hexane and toluene in a packed-bed RFR [1,21–23]. The mathematical model is derived from conservation equations, applied separately to the gas and solid phases. Since both catalyst and inert are monoliths, the proper correlations are used to model mass and heat transport phenomena. The following considerations have been taken into account:

- Total molecular weight of the gas phase is supposed to be constant. This approximation is adequate when the concentration of reactants is low, as in the present case.
- Ideal gas behaviour is assumed for the gas phase.
- Concentration and temperature dependence of the physical properties is taken into account using adequate expressions.
- Gas–solid mass transfer and heat transport are estimated using the expression proposed by Ullah et al. [24] for monoliths.
- Non-ideal flow is considered using the dispersion coefficients in the mass and energy balances. Axial mass and heat dispersion coefficients are determined using the expression proposed by Haynes and Kolaczkowski [25] for laminar flow.
- Mass transfer inside the washcoat layer of the monolith is modelled with the introduction of an effectiveness factor for flat plates [5,24].

The mathematical model is defined by the following set of partial differential equations, where modified Danckwerts boundary conditions are also included to take into account the heat extraction [5]:

- Mass balance for the gas phase:

$$\frac{\partial y_G}{\partial t} = -v_0 \frac{\rho_{G0}}{\rho_G} \frac{\partial y_G}{\partial z} + D_{eff} \frac{\partial^2 y_G}{\partial z^2} - a_G K_G (y_G - y_S) \tag{3}$$

- Energy balance for the gas phase:

$$\frac{\partial T_G}{\partial t} = -v_0 \frac{\rho_{G0}}{\rho_G} \frac{\partial T_G}{\partial z} + \frac{\kappa_{Geff}}{\rho_G C_{PG}} \frac{\partial^2 T_G}{\partial z^2} - \frac{a_G h}{\rho_G C_{PG}} (T_G - T_S) \tag{4}$$

- Mass balance for the solid phase:

$$\frac{\partial y_S}{\partial t} = a_S K_G (y_G - y_S) + \frac{\rho_C \eta(r_m)}{C_{G,tot}} \tag{5}$$

where $(r_m) = -k_m (P_{tot} y_S)^b$ for the catalyst bed, and $(r_m) = 0$ for the inert bed.

- Energy balance for the solid phase:

$$\frac{\partial T_S}{\partial t} = \frac{\kappa_S}{\rho_S C_{PS}} \frac{\partial^2 T_S}{\partial z^2} - \frac{a_S h}{\rho_S C_{PS}} (T_S - T_G) + \frac{\rho_C \eta(r_m) \Delta H_R}{\rho_S C_{PS}} \tag{6}$$

- Reactor boundary conditions:

  - Inlet ($z = 0$):

$$(y_G)_{0^-} = (y_G)_{0^+} - \frac{D_{eff}}{v_0} \left(\frac{\partial y_G}{\partial z} \right)_{0^+},$$

$$(T_G)_{0^-} = (T_G)_{0^+} - \frac{\kappa_{Geff}}{v_0 \rho_{G0} C_{PG}} \left(\frac{\partial T_G}{\partial z} \right)_{0^+} \tag{7}$$

$$\left(\frac{\partial y_S}{\partial z}\right)_{0^+} = \left(\frac{\partial T_S}{\partial z}\right)_{0^+} = 0 \tag{8}$$

◦ Outlet ($z = L_R$):

$$\left(\frac{\partial y_G}{\partial z}\right)_{L_R} = \left(\frac{\partial T_G}{\partial z}\right)_{L_R} = \left(\frac{\partial y_S}{\partial z}\right)_{L_R} = \left(\frac{\partial T_S}{\partial z}\right)_{L_R} = 0 \tag{9}$$

• Boundary conditions at the hot gas extracting point ($z = l$):

◦ For the gas withdrawn from the reactor (methods 1 and 2):

$$\left(\frac{\partial y_G}{\partial z}\right)_{l^-} = \left(\frac{\partial T_G}{\partial z}\right)_{l^-} = 0 \tag{10}$$

◦ For the gas returned to the reactor (only method 2):

$$(y_G)_{l^-} = (y_G)_{l^+} - \frac{D_{eff}}{v_0}\left(\frac{\partial y_G}{\partial z}\right)_{l^+},$$

$$(T_G)_{l^-}^{in} = (T_G)_{l^+} - \frac{\kappa_{Geff}}{v_0 \rho_{G0} C_{PG}}\left(\frac{\partial T_G}{\partial z}\right)_{l^+} \tag{11}$$

where $(T_G)_{l^-}^{in}$ is calculated using one of the following expressions, depending on the variable selected to control the amount of heat extracted from the reactor: the temperature of the gas returning to the reactor (T_C) or the temperature difference in the heat exchanger (ΔT_C):

$$(T_G)_{l^-}^{in} = \begin{cases} \min\{T_C, (T_G)_{l^-}^{out}\} \\ \max\{(T_G)_{l^-}^{out} - \Delta T_C, (T_G)_{0^-}\} \end{cases} \tag{12}$$

As shown in the previous equations, the mathematical model takes into account the heat extraction from the reactor using the adequate boundary conditions for the hot gas extracting point. Furthermore, for the method 1, it is also necessary to introduce the following expression for the reactor gas velocity to consider the decrease in the flow rate, due to the hot gas withdrawal:

$$v_0 = \begin{cases} v_0, & \text{if} \quad z < l \\ (1-\phi)v_0, & \text{if} \quad z > l \end{cases} \tag{13}$$

The kinetic equation describing the catalytic combustion of methane has been determined experimentally in an isothermal fixed-bed reactor. The catalyst has been grinded, in order to ensure intrinsic kinetic behaviour, free of mass transport limitations. The exponent of the kinetic equation (b) has been found to be 1.5. An Arrhenius dependence of the kinetic constant with the temperature is assumed, resulting in the following expression: $k_m = 28.0\exp(-98{,}400/(RT))$.

This model is solved using the method of lines, based on the approximation of the spatial derivatives by finite differences evaluated at different points along the reactor length. The error is reduced by increasing the number of points; in this work a value of 200 points has been found to be enough to ensure a grid independent solution. The resulting system of ordinary differential equations is solved using the MATLAB solver *ode15s*, particularly recommended for stiff problems.

References

[1] D. Fissore, A.A. Barresi, G. Baldi, M.A.G. Hevia, S. Ordóñez, F.V. Díez, Design and testing of small-scale unsteady-state afterburners and reactors, AIChE J. 51 (2005) 1654–1664.

[2] K. Gosiewski, K. Warmuzinski, Effect of the mode of heat withdrawal on the asymmetry of temperature profiles in reverse-flow reactors., Catalytic combustion of methane as a test case, Chem. Eng. Sci. 62 (2007) 2679–2689.

[3] S. Su, A. Beath, H. Guo, C. Mallett, An assessment of mine methane mitigation and utilisation technologies, Prog. Energ. Combust. 31 (2005) 123–170.

[4] K. Gosiewski, Y.Sh. Matros, K. Warmuzinski, M. Jaschik, M. Tanczyk, Homogeneous vs. catalytic combustion of lean methane–air mixtures in reverse-flow reactors, Chem. Eng. Sci. 63 (2008) 5010–5019.

[5] P. Marín, M.A.G. Hevia, S. Ordóñez, F.V. Díez, Combustion of methane lean mixtures in reverse flow reactors: comparison between packed and structured catalyst beds, Catal. Today 105 (2005) 701–708.

[6] D. Edouard, H. Hammouri, X.G. Zhou, Control of a reverse flow reactor for VOC combustion, Chem. Eng. Sci. 60 (2005) 1661–1672.

[7] A.A. Barresi, G. Baldi, D. Fissore, Forced unsteady-state reactors as efficient devices for integrated processes: case histories and new perspectives, Ind. Eng. Chem. Res. 46 (2007) 8693–8700.

[8] M.A.G. Hevia, D. Fissore, S. Ordóñez, A.A. Barresi, F.V. Díez, Combustion of medium concentration CH_4–air mistures in non-stationary reactors, Chem. Eng. J. 131 (2007) 343–349.

[9] Y.S. Matros, G.A. Bunimovich, Reverse-flow operation in fixed bed catalytic reactors, Catal. Rev. 38 (1996) 1–68.

[10] G. Kolios, J. Frauhammer, G. Eigenberger, Autothermal fixed-bed reactor concepts, Chem. Eng. Sci. 55 (2000) 5945–5967.

[11] J. Khinast, A. Gurumoorthy, D. Luss, Complex dynamic features of a cooled reverse-flow reactor, AIChE J. 44 (1998) 1128–1140.

[12] J. Khinast, Y.O. Jeong, D. Luss, Dependence of cooled reverse-flow reactor dynamic on reactor model, AIChE J. 45 (1999) 299–309.

[13] S. Balaji, S. Lakshminarayanan, Heat removal from reverse flow reactors used in methane combustion, Can. J. Chem. Eng. 83 (2005) 695–704.

[14] F. Aubé, H. Sapoundjiev, Mathematical model and numerical simulations of catalytic flow reversal reactors for industrial applications, Comput. Chem. Eng. 24 (2000) 2623–2632.

[15] C. Sapundzhiev, J. Chaouki, C. Guy, D. Klvana, Catalytic combustion of natural gas in a fixed bed reactor with flow reversal, Chem. Eng. Comm. 125 (1993) 171–186.

[16] A. Kushwaha, M. Poirier, R.E. Hayes, H. Sapoundjiev, Heat extraction from a flow reversal reactor in lean methane combustion, Chem. Eng. Res. Des. 83 (2005) 205–213.

[17] K. Gosiewski, Efficiency of heat recovery versus maximum catalyst temperature in a reverse-flow combustion of methane, Chem. Eng. J. 107 (2005) 19–25.

[18] U. Nieken, G. Kolios, G.A. Eigenberger, Fixed-bed reactors with periodic flow reversal: experimental results for catalytic combustion, Catal. Today 20 (1994) 335–350.

[19] M.A.G. Hevia, S. Ordóñez, F.V. Díez, Effect of wall properties on the behaviour of bench-scale reverse flow reactors, AIChE J 52 (2006) 3203–3209.

[20] P. Marín, S. Ordóñez, F.V. Díez, Simplified design methods of reverse flow catalytic combustors for the treatment of lean hydrocarbon–air mixtures, Chem. Eng. Process.: Process Intensification 48 (2009) 229–238.

[21] M.A.G. Hevia, S. Ordóñez, F.V. Díez, Effect of the catalyst properties on the performance of a reverse flow reactor for methane combustion in lean processes, Chem. Eng. J. 129 (2007) 1–10.

[22] M.A.G. Hevia, S. Ordóñez, F.V. Díez, D. Fissore, A.A. Barresi, Design and testing of a control system for reverse-flow catalytic afterburners, AIChE J. 51 (2005) 3020–3027.

[23] P. Marín, S. Ordóñez, F.V. Díez, Combustion of toluene– hexane binary mixtures in a reverse flow catalytic reactor, Chem. Eng. Sci. 63 (2008) 5003–5009.

[24] U. Ullah, S.P. Waldram, Monolithic reactors: mass transfer measurements under reacting conditions, Chem. Eng. Sci. 47 (1992) 2413–2418.

[25] R.E. Hayes, S.T. Kolaczkowski, Introduction to Catalytic Combustion, Gordon and Breach Science Publishers, Amsterdam, 1997.